

Effect of Non-Resonant Gain Structure Design in Membrane External-Cavity Surface-Emitting Lasers

Philipp Tatar-Mathes¹, Hoy-My Phung¹, Aaron Rogers¹, Patrik Rajala¹, Sanna Ranta¹,
Mircea Guina², *Member, IEEE*, and Hermann Kahle²

Abstract—The operation of a semiconductor membrane external-cavity surface-emitting laser (MECSEL) employing a gain membrane with a cavity design, which is non-resonant regarding the two semiconductor-heat-spreader interfaces, is presented. The MECSEL delivers watt-level output power, in line with state-of-the-art results. The study provides new evidence that the design criteria of a MECSEL gain region are significantly relaxed compared to active regions employing distributed Bragg reflectors, for which the field distribution is set by the Bragg condition leading to tight tolerances for positioning of the emitting quantum structures. The study has relevance especially for the development of mode-locked MECSELS by minimizing the impact of defective Fabry-Pérot micro-cavity effects due to reflections between the semiconductor gain structure and the two heat-spreader elements placed on each side of the semiconductor membrane.

Index Terms—MECSEL, non-resonant, vertical emitter.

I. INTRODUCTION

AMONG vertically emitting semiconductor lasers, MECSELS [1], [2] stand out due to the absence of monolithically integrated distributed Bragg reflectors (DBRs). In terms of general performance, both types of optically pumped surface emitting semiconductor lasers with external cavity, i.e. vertical-external-cavity surface-emitting lasers

(VECSELS) [3], [4], and MECSELS, can deliver watt-level diffraction limited beams in a broad wavelength range benefiting from excellent thermal management enabled by the thin-disk gain architecture. Yet, the MECSEL allows for improved thermal management linked to the use of two heat-spreaders in immediate proximity of the active region [5], [6]. Additional power scaling can be obtained by employing double side [7] or multi-pass pumping [8]. This is enabled by the optical access to both sides of the active region due to the absence of substrate and DBR. Furthermore, the lack of DBRs relaxes the material related restrictions, which make for example InP based DBRs extremely difficult to realize. This feature has been already exploited in MECSELS operating at the short red wavelengths, i.e. 660 nm [2] as well as long infrared wavelengths near 1.5 μm to 1.7 μm spectral range [9], [10]. On the same line, the ability of MECSELS to achieve a broader wavelength tunability [11] and to implement a design optimized towards mode-locking operation [12] has been also demonstrated. In terms of thermal management, the expected benefits of using two heat-spreaders [5], have been recently experimentally proven to be typically larger than a factor of two [13] when using two instead of one single heat-spreader. Consequently, the double heat-spreader approach has become a standard in MECSELS [14], [15]. In fact, this has opened the possibility to use lower cost SiC heat-spreaders instead of much more expensive diamond alternative, which may be also affected by birefringence. On the other hand, the use of two heat-spreaders induces additional unwanted etalon effects associated with the multitude of semiconductor-heat-spreader and heat-spreader-air interfaces (see Fig. 1), with detrimental effects on tuning and wavelength selection ability. In mode-locked VECSELS, it is a well-known practice to facilitate wedged heat spreaders when used inside the cavity to avoid this effect [16]. However, when moving towards a mode-locked MECSEL, the proposed design consideration should be taken into account in addition to wedged heat spreaders. We should also note that additional tuning limitations may arise from the fact that the majority of VECSEL structures, and to the best of our knowledge all MECSEL structures reported so far, employ a so called resonant periodic gain (RPG) gain structure design [17], leading to gain enhancement owing to the Fabry-Pérot microcavity effect. In practice this means that the thickness of the active region is a multiple of half-wavelength, forming a standing wave pattern inside the structure (see Fig. 1). This is advantageous for increasing the modal gain and thus reducing the threshold and/or the

Manuscript received 23 February 2023; revised 26 March 2023; accepted 16 April 2023. Date of publication 25 April 2023; date of current version 9 May 2023. This work was supported in part by the Academy of Finland under Grant 326455, in part by the Academy of Finland Flagship on Photonics Research and Innovation (PREIN) Program under Grant 320165, in part by the Horizon 2020 Marie Skłodowska-Curie Actions–Next Generation of Tunable LASers for Optical Coherence Tomography (NetLas) under Grant 860807, in part by the Magnus Ehrnrooth Foundation, and in part by the Finnish Foundation for Technology Promotion. (*Corresponding author: Philipp Tatar-Mathes.*)

Philipp Tatar-Mathes, Aaron Rogers, Patrik Rajala, Sanna Ranta, and Mircea Guina are with the Optoelectronics Research Centre (ORC), Physics Unit/Photonics, Faculty of Engineering and Natural Sciences, Tampere University, 33720 Tampere, Finland (e-mail: philipp.tatar-mathes@tuni.fi; aaron.rogers@tuni.fi; patrik.rajala@tuni.fi; sanna.ranta@tuni.fi; mircea.guina@tuni.fi).

Hoy-My Phung was with the Optoelectronics Research Centre (ORC), Physics Unit/Photonics, Faculty of Engineering and Natural Sciences, Tampere University, 33720 Tampere, Finland. She is now with Robert Bosch GmbH, 71272 Renningen, Germany.

Hermann Kahle was with the Optoelectronics Research Centre (ORC), Physics Unit/Photonics, Faculty of Engineering and Natural Sciences, Tampere University, 33720 Tampere, Finland. He is now with the Center for Optoelectronics and Photonics Paderborn (CeOPP), Institute for Photonic Quantum Systems (PhoQS), Paderborn University, 33098 Paderborn, Germany (e-mail: hermann.kahle@uni-paderborn.de).

Color versions of one or more figures in this letter are available at <https://doi.org/10.1109/LPT.2023.3270404>.

Digital Object Identifier 10.1109/LPT.2023.3270404

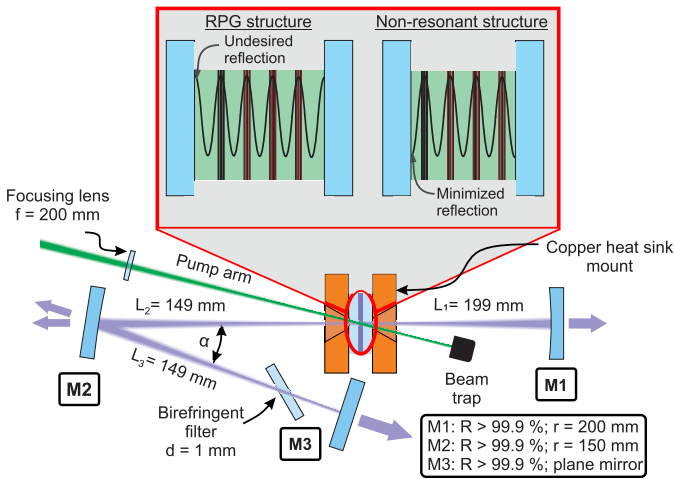


Fig. 1. Schematic illustration of a MECSELS cavity architecture. The upper zoom-out pictures illustrate the standing wave field distribution in a typical RPG structure (left) and a non-resonant gain structure configuration studied in this letter (right). Field intensities are normalized to emphasize the differences.

ability to tolerate intracavity losses. On the other hand, when considering a design for the active region that can be tuned across a broad wavelength range, i.e. tens to about 100 nm [18], the resonant condition is fulfilled for a much smaller spectral band. From this standpoint, the main purpose of this study is to investigate the operation of an anti-resonant MECSEL gain structure design, which has an inherent benefit in minimizing reflection at the semiconductor-heat-spreader interfaces for a certain wavelength range, thus potentially being more favorable for mode-locking operation.

II. FABRICATION

The structure was grown on an undoped $325 \mu\text{m}$ thick GaAs wafer oriented in the $(100) \pm 0.5^\circ$ plane using a V80H-10 VG Semicon solid source molecular beam epitaxy reactor. First, a 100 nm thick GaAs buffer layer was grown, followed by a 100 nm thick AlAs etch stop layer. The etch stop layer was followed by a 470 nm thick active region, consisting of twelve compressively strained GaInAsP quantum wells (QWs) optimized for emission at 800 nm. The QWs had a thickness of 6 nm and were arranged in four groups comprising of three QWs each. They were embedded within tensile strained GaInP barriers and spacer layers. For preventing charge carrier diffusion to the outer semiconductor facets, 20 nm thick AlGaInP layers enclose the active region. Similar to RPG structures, the QWs were placed periodically at a distance corresponding to the anti-nodes of the standing wave formed by the laser cavity. Yet again, compared to a typical gain structure design, the overall thickness is an odd number of quarter-wavelength thus having antinodes at the semiconductor-heat-spreader interfaces. A scanning electron microscopy (SEM) image of the unprocessed gain structure revealing the thickness and the distribution of the QWs with respect to the optical field is shown in Fig. 2. As it can be easily retrieved from Fig. 2, the design favors operation at phase conditions that correspond to anti-resonant operation (red solid line), i.e., for the phase corresponding to resonant condition

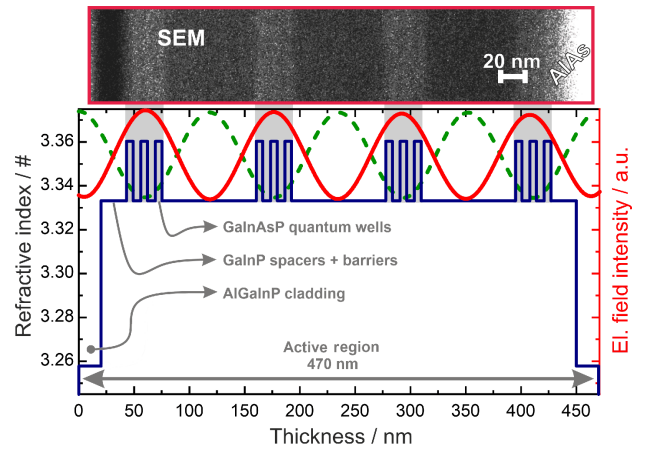


Fig. 2. SEM image of the unprocessed sample (top). Refractive index of the active region with the simulated intensity of the standing wave electric field distribution in red plotted over membrane thickness (bottom).

(green dashed line), the QWs would be placed in the antinodes of the field distribution. This can be quantitatively explained by calculating the gain enhancement factor Γ_{enh} following the model of Corzine et al. [19]. Thus $\Gamma_{\text{enh}} \approx 0.15$ for a phase condition corresponding to resonant operation, while it is $\Gamma_{\text{enh}} \approx 1.85$ for the phase condition corresponding to anti-resonant operation, which is then favored in terms of net modal gain.

III. CHARACTERIZATION

To use the active region as a gain membrane in a MECSEL, the substrate was removed wet chemically down to the AlAs process layer using a mixture of ammonium hydroxide and hydrogen peroxide. The process layer was removed with an HF solution. The obtained membrane was sandwiched between two transparent uncoated 4H SiC heat-spreader pieces and mounted in a copper heat sink. During all measurements, the copper heat sink was kept at a fixed temperature of 18°C . We used a Coherent Verdi V18 for optical excitation of the sample. A $f = 200 \text{ mm}$ lens was used to focus the pump beam through the aperture (1.5 mm in diameter) in the copper heat sink onto one of the sample's sides under an angle of incidence of approximately 14° . Power characteristics (see Fig. 3a) of the MECSEL were measured in a linear cavity. One mirror was highly reflective (HR) with a radius of curvature of 75 mm, the other mirror had a reflectivity of 97% with a radius of curvature of 100 mm, the total cavity length adds up to 174 mm and the gain sandwich was placed in the waist of the cavity mode. The cavity mode diameter in the gain sandwich was simulated to be about $(64 \pm 6) \mu\text{m}$. The pump spot diameter was calculated to be $(80 \pm 4) \mu\text{m}$, which is in good agreement with the recommended diameter relation for stable single-mode operation [20]. The power measurement was plotted with respect to absorbed pump power, obtained by measuring incident pump power and subtracting the reflected and transmitted power. An output power of more than 1.0 W could be reached.

Tuning measurements (see Fig. 3b) were performed in a V-shaped cavity configuration as shown in Fig. 1. One HR mirror with 200 mm radius of curvature and one HR with

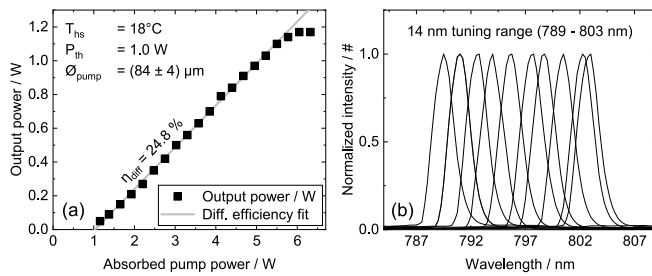


Fig. 3. Performance characteristics given by (a) the power performance and (b) the tuning range of the presented structure.

150 mm were used, such as a plane HR mirror. The overall cavity length added up to 497 mm. A 1 mm thick birefringent filter was inserted at Brewster's angle into the cavity as a tuning element. The laser was tuned from 789 nm to 803 nm. These results are comparable to previous work from Phung et al. [6] for similar wavelength region in the same material system. That structure consisted of 3×3 GaInAsP QW region with a RPG design. We note that for operation at 825 nm, the charge carrier confinement is significantly better.

IV. CONCLUSION

The operation of a MECSEL based on a gain structure with an anti-resonant design was investigated. Lasing with an output power comparable to performance of an RPG design at similar wavelength region is demonstrated. Benefiting from a gain enhancement factor that is at least ten-fold higher for wavelengths corresponding to anti-resonant operation than for resonant operation, lasing is promoted at wavelengths for which the reflections at the semiconductor-heat-spreader interface are minimized. This experimentally demonstrates the enhanced flexibility and error tolerance in fabricating MECSEL gain structures; owing to the absence of a monolithically integrated DBR the mode distribution will align to ensure the highest model gain and lead to similar performance for both anti-resonant and resonant operation. The design may be advantageous for mode-locking conditions by reducing spectral filtering effects and thus avoid perturbations in the mode-locking mechanism.

REFERENCES

- [1] Z. Yang, A. R. Albrecht, J. G. Cederberg, and M. Sheik-Bahae, "Optically pumped DBR-free semiconductor disk lasers," *Opt. Exp.*, vol. 23, no. 26, pp. 33164–33169, 2015, doi: [10.1364/OE.23.033164](https://doi.org/10.1364/OE.23.033164).
- [2] H. Kahle et al., "Semiconductor membrane external-cavity surface-emitting laser (MECSEL)," *Optica*, vol. 3, no. 12, p. 1506, Dec. 2016, doi: [10.1364/OPTICA.3.001506](https://doi.org/10.1364/OPTICA.3.001506).
- [3] M. Kuznetsov, F. Hakimi, R. Sprague, and A. Mooradian, "High-power (>0.5-W CW) diode-pumped vertical-external-cavity surface-emitting semiconductor lasers with circular TEM₀₀ beams," *IEEE Photon. Technol. Lett.*, vol. 9, no. 8, pp. 1063–1065, Aug. 1997, doi: [10.1109/68.605500](https://doi.org/10.1109/68.605500).
- [4] M. Guina, A. Rantamäki, and A. Härkönen, "Optically pumped VECSELS: Review of technology and progress," *J. Phys. D, Appl. Phys.*, vol. 50, no. 38, Sep. 2017, Art. no. 383001, doi: [10.1088/1361-6463/aa7bfd](https://doi.org/10.1088/1361-6463/aa7bfd).
- [5] V. Iakovlev et al., "Double-diamond high-contrast-gratings vertical external cavity surface emitting laser," *J. Phys. D, Appl. Phys.*, vol. 47, no. 6, 2014, Art. no. 065104, doi: [10.1088/0022-3727/47/6/065104](https://doi.org/10.1088/0022-3727/47/6/065104).
- [6] H.-M. Phung, H. Kahle, J.-P. Penttinen, P. Rajala, S. Ranta, and M. Guina, "Power scaling and thermal lensing in 825 nm emitting membrane external-cavity surface-emitting lasers," *Opt. Lett.*, vol. 45, no. 2, pp. 547–550, 2020, doi: [10.1364/OL.382377](https://doi.org/10.1364/OL.382377).
- [7] H. Kahle et al., "Comparison of single-side and double-side pumping of membrane external-cavity surface-emitting lasers," *Opt. Lett.*, vol. 44, no. 5, pp. 1146–1149, Mar. 2019, doi: [10.1364/OL.44.001146](https://doi.org/10.1364/OL.44.001146).
- [8] D. Priante et al., "Demonstration of a 20-W membrane-external-cavity surface-emitting laser for sodium guide star applications," *Electron. Lett.*, vol. 57, no. 8, pp. 337–338, 2021, doi: [10.1049/el12.12008](https://doi.org/10.1049/el12.12008).
- [9] H.-M. Phung et al., "Quantum dot membrane external-cavity surface-emitting laser at 1.5 μm," *Appl. Phys. Lett.*, vol. 118, no. 23, Jun. 2021, Art. no. 231101, doi: [10.1063/5.0053961](https://doi.org/10.1063/5.0053961).
- [10] B. Jezewski et al., "Membrane external-cavity surface-emitting laser emitting at 1640 nm," *Opt. Lett.*, vol. 45, no. 2, pp. 539–542, 2020, doi: [10.1364/OL.381531](https://doi.org/10.1364/OL.381531).
- [11] Z. Yang, A. R. Albrecht, J. G. Cederberg, and M. Sheik-Bahae, "80 nm tunable DBR-free semiconductor disk laser," *Appl. Phys. Lett.*, vol. 109, no. 2, Jul. 2016, Art. no. 022101, doi: [10.1063/1.4958164](https://doi.org/10.1063/1.4958164).
- [12] M. Sheik-Bahae, "Analysis of MECSEL mode-locking," in *Proc. SPIE*, vol. 11984, pp. 29–36, Mar. 2022, doi: [10.1117/12.2610991](https://doi.org/10.1117/12.2610991).
- [13] H.-M. Phung et al., "Thermal behavior and power scaling potential of membrane external-cavity surface-emitting lasers (MECSELS)," *IEEE J. Quantum Electron.*, vol. 58, no. 2, pp. 1–11, Apr. 2022, doi: [10.1109/JQE.2022.3147482](https://doi.org/10.1109/JQE.2022.3147482).
- [14] S. Mirkhanov et al., "DBR-free semiconductor disc laser on SiC heat-spreader emitting 10.1 W at 1007 nm," *Electron. Lett.*, vol. 53, no. 23, pp. 1537–1539, Nov. 2017, doi: [10.1049/el.2017.2689](https://doi.org/10.1049/el.2017.2689).
- [15] Z. Yang et al., "16 W DBR-free membrane semiconductor disk laser with dual-SiC heatspreader," *Electron. Lett.*, vol. 54, no. 7, pp. 430–432, 2018, doi: [10.1049/el.2018.0101](https://doi.org/10.1049/el.2018.0101).
- [16] J. Rautaiainen et al., "1.3-μm mode-locked disk laser with wafer fused gain and SESAM structures," *IEEE Photon. Technol. Lett.*, vol. 22, no. 11, pp. 748–750, Jun. 2010, doi: [10.1109/LPT.2010.2045494](https://doi.org/10.1109/LPT.2010.2045494).
- [17] M. Y. A. Raja et al., "Resonant periodic gain surface-emitting semiconductor lasers," *IEEE J. Quantum Electron.*, vol. 25, no. 6, pp. 1500–1512, Jun. 1989, doi: [10.1109/3.29287](https://doi.org/10.1109/3.29287).
- [18] P. Rajala et al., "Design and characterization of MECSELS for widely tunable (>25 THz) continuous wave operation," in *Proc. SPIE*, vol. 11984, Mar. 2022, Art. no. 1198404, doi: [10.1117/12.2610649](https://doi.org/10.1117/12.2610649).
- [19] S. W. Corzine, R. S. Geels, J. W. Scott, R.-H. Yan, and L. A. Coldren, "Design of Fabry-Perot surface-emitting lasers with a periodic gain structure," *IEEE J. Quantum Electron.*, vol. 25, no. 6, pp. 1513–1524, Jun. 1989, doi: [10.1109/3.29288](https://doi.org/10.1109/3.29288).
- [20] A. Laurain, J. Hader, and J. V. Moloney, "Modeling and optimization of transverse modes in vertical-external-cavity surface-emitting lasers," *J. Opt. Soc. Amer. B, Opt. Phys.*, vol. 36, no. 4, pp. 847–854, Apr. 2019, doi: [10.1364/JOSAB.36.000847](https://doi.org/10.1364/JOSAB.36.000847).